Journal of Research and Applications in Mechanical Engineering
ISSN: 2229-2152 (Print); 2697-424x (Online)
(2023) Vol. 11, No. 1, Paper No. JRAME-23-11-001
[DOI: 10.14456/jrame.2023.1]

Research Article

A Light Amphibious Airplane's Drop Test Identification Using Multi Kernel Least Square Support Vector Machines

S. Chinvorarat*
B. Watjatrakul
P. Nimdum
T. Sangpet
P. Vallikul
Department of Mechanical and Aerospace Engineering
King Mongkut's University of Technology North Bangkok, Bangkok 10800, Thailand

Received 19 January 2023
Revised 9 March 2023
Accepted 20 March 2023

Abstract:
This article uses multi-kernel least square support vector machines to determine the drop test dynamics for a light amphibious aircraft's stock strut landing gear. The kernel function to assess system nonlinearity is the Gaussian radial basis. The suggested multi-kernel LS-SVM model has shown to provide more accurate displacement output estimation than the traditional LS-SVM model, with RMSE values of 0.21766 and 0.062726 for the strut and wheel of the landing gear, respectively. The drop test of the light amphibious aircraft is conducted to validate the identification capabilities.

Keywords: *Multi-kernel LS-SVM, Gaussian radial basis, Landing gear drop dynamics, Light amphibious airplane*

1. Introduction

The landing gear of an aircraft is designed to protect the airframe and the passengers from harm during landings, whether they are normal or emergency situations [1]. Landing gear of all varieties must be tailored to each specific kind of airplane [2]. Certain light sport aircraft have an MTOW limit of 650 kg for water airplanes. The landing gear must pass a static drop test in compliance with ASTM F-2245 - Standard for Design and Operation of a Light-Sport Aircraft, proving its durability and adequate dynamic reaction to guarantee the aircraft's steadiness and safety during take-off and landing. Or, alternatively, drop test dynamics of the undercarriage must be shown using experimental and analytical methods to verify the original design's accuracy. The designer may learn about the landing gear's dynamic behavior by analyzing the drop test dynamic model.

Following its creation by Vapnik [3, 4] in 1979 and 1995, support vector machines (SVMs) have since been a standard part of machine learning studies all around the globe [5]. The support vector machine (SVM) is a basic class of supervised learning techniques for data classification and regression. By finding a hyperplane approximation for the training function, the SVM is able to effectively transform a nonlinear training process to a high-dimensional domain when using the appropriate kernel function. Because of its potential to classify data into several categories without resorting to real data transformation, hyperplane classification may save time and effort. Therefore, the SVM may represent any non-linear function by mapping the nonlinear signals into a hyperplane and then using a linear function to solve for the relevant parameters. Adding least squares to SVM improved linear regression performance, as shown by the work of Suykens et al. [6, 7].

*Corresponding author: S. Chinvorarat
E-mail address: sinchai.c@eng.kmutnb.ac.th

Nonlinear dynamic systems were detected using LS-SVM by Wang et al. in 2004. The LS-SVM technique for realtime identifying of nonlinear systems was studied by Resendiz et al. [8]. To determine a nonlinear undercarriage models in the frequency response, Viana et al. [9] used optimization techniques taken from nature. An approach for nonlinear identification using multi-kernel least support was created by Tarhouni et al. [10], although it requires just two kernel functions. The landing gear coefficient of discharge was computed by Ding et al. [11] using a dynamics mathematical equation of motion and a study of CFD findings on a model with a dynamic drop. Recently, Chinvorarat et al. [12-15] introduced the Weiner identification model which is based on little input to accurately identify the dynamics of a light amphibious aircraft's drop test. This research has however proposed a formulation for the multi-kernel LS-SVM method and identified the landing gear wheel and strut of the light amphibious airplane.

The goal of this research was to use the multi-kernel LS-SVM to analyze drop dynamics of an undercarriage shock strut in compliance with ASTM F-2245 [16]. Section 2 explains how to build a model of the shocks strut landing gear of a lightweight amphibious aircraft. Section 3 discusses the least square support vector machines (LS-SVMs) and its uses in nonlinear system identification. Model, method, and mathematical formulation for the multi-kernel LS-SVM are presented in Section 4. In Section 5, we detail the methodology behind our drop test experiment, provide the results of our simulation of the dropping dynamics and its identification using the proposed model and alternative models, and analyze the implications of these findings. The last part includes the summary and analysis.

2. Shock Strut Model

Figure 1 depicts a lightweight amphibious aircraft that has been built to improve safety and stability during normal or emergencies runway landings by using foldable main gears and a shock-absorbing strut. The shocks strut is shown in detail in Figs. 2 and 3, which illustrate several diagrams of the component. Aluminum, which has the dual benefits to be lightweight and manageable, is used for much of a shock strut's manufacture because to these qualities. The strut has a pressurized hydraulic fluid upper chamber and a pressured nitrogen gas bottom chamber. There are two flow-regulating valves, one at each piston's tip. Each valve regulates oil flow in one of two directions; the larger orifice of the first valve allows for more flow during extensions, while the smaller aperture of the second valve allows for greater flow during retraction. Hydraulic pressure drops across the aperture slows the struts moving, and the resulting fluid turbulence effectively disperses impact energy. It is the acceleration of the bottom part of the fuselage caused by the force created within the strut that causes the tire to deform (Milwizky and Cook [17]). Strut and tire interactions must be considered when analyzing the system as a whole.

Fig. 1. A small, shock-strut-equipped amphibious aircraft.

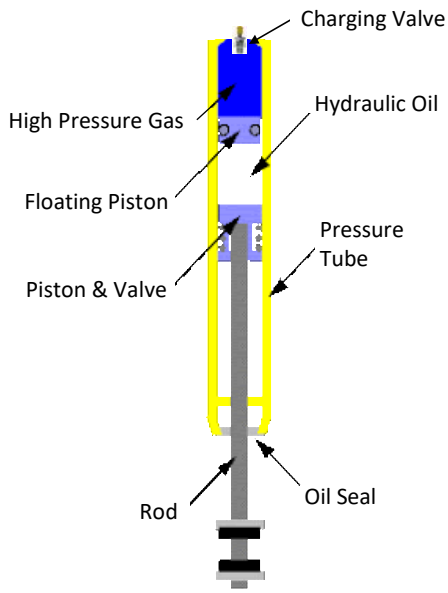

Fig. 2. Shock strut diagrammatic representation.

Axial force due to hydraulic resistance, nitrogen gas compression, and internal friction may be calculated using the following formula:

$$\begin{aligned} F_s &= (p_h - p_a)\left(A_1 - A_p\right) + p_a A_2 + F_f \\ &= (p_h - p_a)A_h + p_a A_a + F_f \\ &= F_h + F_a + F_f \end{aligned} \tag{1}$$

where

$$F_h = \frac{\dot{s}}{|\dot{s}|}\frac{\rho A_h^3}{2(C_d A_n)^2}\dot{s}^2 \tag{2}$$

$$F_a = p_{a_0} A_a \left(\frac{V_0}{V_0 - A_a s}\right)^n \tag{3}$$

$$F_f = \frac{\dot{s}}{|\dot{s}|}(\mu_1|F_1| + \mu_2|F_2|) \tag{4}$$

Tire compression during landing may be described as a vertical response force, and this force can be calculated using:

$$F_v = \left(1 + C_T\dot{\delta}\right)f(\delta) \tag{5}$$

Finally, the landing gear equation of motion, ignoring wheel rotation, is written as follows:

$$m_1\ddot{z}_1 = m_1 g - \left(F_h + F_a + F_f\right)\cos\theta \tag{6}$$

$$m_2\ddot{z}_2 = m_2 g - \left(F_h + F_a + F_f\right)\cos\theta - F_v \tag{7}$$

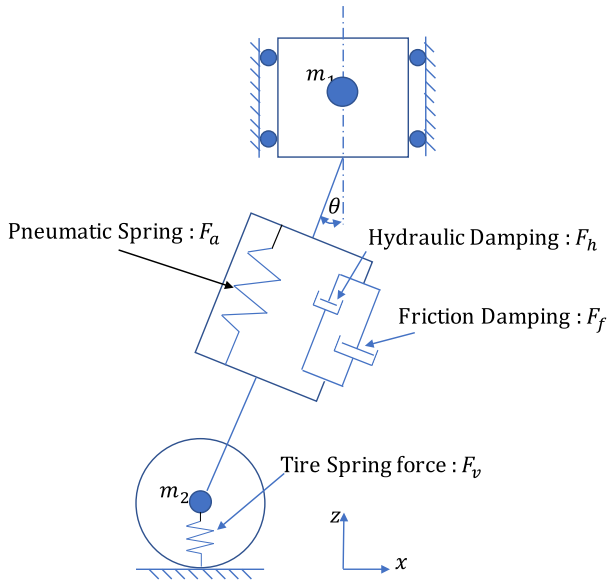

Fig. 3. Landing gear diagram schematic.

An internal axial force drives the bottom part of the strut and the aircraft body forward via the tyre's compression and distraction. Because hydrodynamic force, compressed air force, friction coefficient, and tyre response force are fundamentally nonlinear functions, the dynamic properties of the undercarriage have a low degree of predictability and are difficult to forecast in general. In addition to calculating the landing gear's equation of motion using equations (6) and (7), a workable nonlinear identification model is offered for detecting and assessing the landing gear's dynamic response. Nonlinear identification is presented, and its model response is far more precise than that obtained by using the conventional governing equation of motion.

3. LS-SVM Regression principle

SVMs, developed by Vladimir Vapnik in the late 1970s and based on statistical learning theory, were first employed for regression and pattern recognition. The SVM structure is particularly remarkable since it delivers a hyperplane classifier solution for a complicated model while still being comprehensible as a linear technique. In 2D, the SVM divides the training set into two classes, class +1 and class -1. In recent years, SVM and its variants have been applied to estimate nonlinear models (Wang et al. [18]).

Support Vector Regression (SVR) may be used to model any nonlinear function and employs the same approach as support vector machines by categorizing the output of the function as $y \in \mathrm{R}$ rather than $y \in \{\pm 1\}$. The accuracy of the identified regression model is contingent upon the kernel function used, the quantity of training data, and the complexity of the nonlinear function itself.

Let nonlinear dynamic systems with input u and output y are described in the discrete-time by:

$$y(k) = f\big(\mathrm{x}(k)\big) \tag{8}$$

where $(.)$ is a nonlinear function, $y(k) \in \mathbb{R}$ denotes the output at the time instant k, and $\mathrm{x}(k)$ is the regressor vector written as:

$$\mathrm{x}(k) = [y(k-1) \dots y\big(k-n_y\big)\ u(k) \dots u(k-n_u)^T \tag{9}$$

Where n_u is dynamic inputs order, and n_y is dynamic outputs order. In reality, the outputs are normally corrupted by some measurement noise, which we can rewrite the nonlinear function as:

$$y(k) = f\big(\mathrm{x}(k)\big) + e(k) \tag{10}$$

where $e(k)$ denotes the measurement noise and is typically modelled by Gaussian noise with zero mean and finite variance. To include the functional estimates provided by least square support vector machines (LS-SVM), the structure of the static nonlinearity is assumed: (Jing, S., [19]).

$$f(x) = w^T \varphi(x) + d \tag{11}$$

Data is mapped from one feature space into a higher-dimensional feature space by use of the feature map $\varphi(.)$, where $w \in \mathbb{R}$ and $d \in \mathbb{R}$ are unknown parameters. Using the well-known Least Square (LS) for function approximation by means of SVM, the approximation issue may then be expressed as an optimization problem known as LS-SVM. The usual optimization issue may therefore be stated as follows.

$$\min_{w,d,e_k} \mathcal{F}(w, e_k) = \frac{1}{2}\|w\|^2 + \frac{\gamma}{2}\sum e_k^2 \tag{12}$$

$$s.t.$$

$$y_k = w^T \varphi(x) + d + e_k, \quad \forall \mathrm{t} = 1, .., \mathrm{N} \tag{13}$$

Where $\|.\|$ is the standard Euclidian norm in $\mathbb{R}^n$, and γ is the penalty term. In order to resolve the constraint optimization issue, the Lagrangian may be constructed as follows.

$$\mathcal{L}(w, d, e_k, \alpha) = \mathcal{F}(w, e_k) - \sum_{k=1}^{N} \alpha_k (w^T \varphi(x_k) + d + e_k - y_k) \tag{14}$$

Where α_k is a Lagrange multiplier, the following equations are derived from the Karush-Kuhn-Tucher (KKT) conditions.

$$\frac{\partial \mathcal{L}}{\partial w} = 0 \Longrightarrow w = \sum_{k=1}^{N} \alpha_t \, \varphi(x_k) \tag{15}$$

$$\frac{\partial \mathcal{L}}{\partial d} = 0 \Longrightarrow \sum_{k=1}^{N} \alpha_k = 0 \tag{16}$$

$$\frac{\partial \mathcal{L}}{\partial e_k} = 0 \Longrightarrow \alpha_k = \gamma e_k, \qquad k = 1, \dots, N \tag{17}$$

$$\frac{\partial \mathcal{L}}{\partial \alpha_k} = 0 \Longrightarrow y_k = w^T \varphi(x_k) + d + e_k \tag{18}$$

We substitute (15), (17) into (18), obtain the following

$$\frac{\partial \mathcal{L}}{\partial \alpha_k} = 0 \Longrightarrow y_k = w^T \varphi(x_k) + d + e_k \tag{19}$$

Rewrite (16) and (19) as a set of linear equations in the following

$$\begin{bmatrix} 0 & 1_{\mathrm{N}}^{\mathrm{T}} \\ 1_{\mathrm{N}} & \Omega + \gamma^{-1} \mathrm{I}_{\mathrm{N}} \end{bmatrix} \begin{bmatrix} \mathrm{d} \\ \alpha \end{bmatrix} = \begin{bmatrix} 0 \\ \mathrm{Y} \end{bmatrix} \tag{20}$$

Where $\Omega = \varphi(x_t)^T \varphi(x_k) = K(x_t, x_k)$ is a positive definite kernel matrix that represents the inner product of the data in the feature space. This phenomenon, referred to as the "Kernel Trick," happens when data are not linearly separable in input space but are in fact linearly separable in feature space. Kernel function is a fundamental component of SVM that, when chosen correctly, delivers the best results. The LS-SVM will offer the output and utilize it.

$$y(x) = \sum_{k=1}^{N} \alpha_k K(x_t, x_k) + d, \;\; t = 1, \dots, N \tag{21}$$

Where α_k and $d \in \mathbb{R}$ are solutions of (20), x_k is training data, and x_t is the input vector.

4. Multi kernel LS-SVM

Assume the system dynamics is given by (8), where the nonlinear function is given by

$$y(k) = f\big(x(k)\big) = a_0 y_{k-1} + b_0 y_{k-2} + c_1 u_{k-1} + c_2 u_{k-2} + w^T \varphi(x_k) + d + e_k \tag{22}$$

Instead of using a single kernel for nonlinear function, one could utilize four multiple kernels to model nonlinear function as shown in Figure 4 (Sonnenburg et al. [20]).

$$\begin{aligned} y(k) = f\big(x(k)\big) = {} & a_0 y_{k-1} + b_0 y_{k-2} + c_1 u_{k-1} + c_2 u_{k-2} + f_1(u_{k-1}, y_{k-1}) + f_2(u_{k-2}, y_{k-1}) + f_3(u_{k-1}, y_{k-2}) \\ & + f_4(u_{k-2}, y_{k-2}) + e_k \end{aligned} \tag{23}$$

Where

$f_1(u_{k-1}, y_{k-1}) = w_{a1}^T \varphi(x_{a1}(k)) + d_1$
$f_2(u_{k-2}, y_{k-1}) = w_{a2}^T \varphi(x_{a2}(k)) + d_2$
$f_3(u_{k-1}, y_{k-2}) = w_{b1}^T \varphi(x_{b1}(k)) + d_3$
$f_4(u_{k-2}, y_{k-2}) = w_{b2}^T \varphi(x_{b2}(k)) + d_4$

where

$$x_{a1} = \begin{bmatrix} u_k \\ y_{k-1} \end{bmatrix},\ x_{a2} = \begin{bmatrix} u_{k-2} \\ y_{k-1} \end{bmatrix},\ x_{b1} = \begin{bmatrix} u_{k-1} \\ y_{k-2} \end{bmatrix},\ x_{b2} = \begin{bmatrix} u_{k-2} \\ y_{k-2} \end{bmatrix}$$

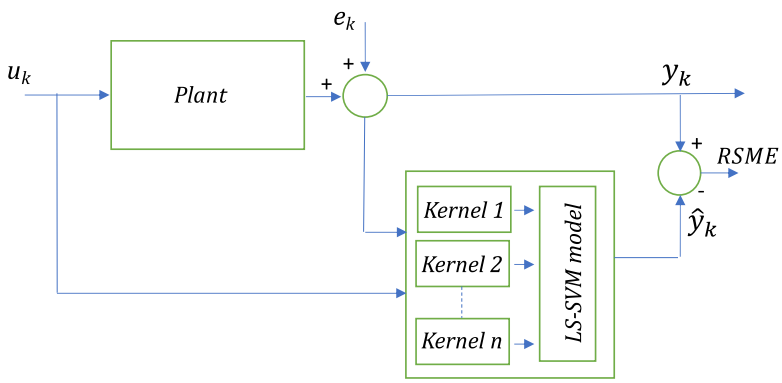

Fig. 4. Multi Kernel LS-SVM identification model.

Rewrite (23)

$$\begin{aligned} y(k) = f\big(x(k)\big) = {} & a_0 y_{k-1} + b_0 y_{k-2} + c_1 u_{k-1} + c_2 u_{k-2} + w_{a1}^T \varphi(x_{a1}(k)) + w_{a2}^T \varphi(x_{a2}(k)) + w_{b1}^T \varphi(x_{b1}(k)) \\ & + w_{b2}^T \varphi(x_{b2}(k)) + d + e_k, \qquad k = r, \dots, N \end{aligned} \tag{24}$$

Where. $d = d_1 + d_2 + d_3 + d_4$

To obtain the optimal points, the standard optimization problem can be formulated as

$$\min_{w_x, e_k} \mathcal{F}(w, e_k) = \frac{1}{2} \sum_x w_x^{\mathrm{T}} w_x + \frac{\gamma}{2} \sum_{k=r}^{N} e_k^2$$

$s.t.$

$$\begin{aligned} y(k) = {} & a_0 y_{k-1} + b_0 y_{k-2} + c_1 u_{k-1} + c_2 u_{k-2} + w_{a1}^T \varphi\big(x_{a1}(k)\big) + w_{a2}^T \varphi\big(x_{a2}(k)\big) + w_{b1}^T \varphi\big(x_{b1}(k)\big) \\ & + w_{b2}^T \varphi\big(x_{b2}(k)\big) + d + e_k, \qquad k = r, \dots, N \end{aligned} \tag{25}$$

and

$$\sum_{k=1}^{N} w_x^{\mathrm{T}} \varphi\big(x_x(k)\big) = 0, \quad x = a_1, a_2, b_1, b_2 \tag{26}$$

In order to resolve the constraint optimization issue, the Lagrangian may be constructed as follows.

$$\begin{aligned}\mathcal{L}(w, \mathrm{a}, \mathrm{b}, \mathrm{c}, d, e_k, \alpha, \beta) &= \mathcal{F}(w, e_k) - \sum_{k=r}^{N} \alpha_k (a_0 y_{k-1} + b_0 y_{k-2} + c_1 u_{k-1} + c_2 u_{k-2} + w_{a1}^T \varphi\big(x_{a1}(k)\big) + w_{a2}^T \varphi\big(x_{a2}(k)\big) \\ &+ w_{b1}^T \varphi\big(x_{b1}(k)\big) + w_{b2}^T \varphi\big(x_{b2}(k)\big) + d + e_k - y_k) - \sum_{x=a_1,a_2,b_1,b_2} \beta_x \sum_{k=1}^{N} w_x^{\mathrm{T}} \varphi\big(x_x(k)\big)\end{aligned} \tag{27}$$

Where α_k, β_x are lagrange multipliers, the following equations are derived from the Karush-Kuhn-Tucher (KKT) conditions.

$$\frac{\partial \mathcal{L}}{\partial w_x} = 0 \Longrightarrow w_x = \sum_{k=r}^{N} \alpha_k \, \varphi(x_k) + \beta_x \sum_{k=1}^{N} \varphi(x_k),$$
$$x = a_0, b_0, c_1, c_2 \tag{28}$$

$$\frac{\partial \mathcal{L}}{\partial a_0, b_0, c_1, c_2} = 0 \Longrightarrow \sum_{k=r}^{N} \alpha_k \, y(k-i) = 0, \quad i = 1,2$$
$$\sum_{k=r}^{N} \alpha_k \, u(k-i) = 0, \quad i = 1,2 \tag{29}$$

$$\frac{\partial \mathcal{L}}{\partial d} = 0 \Longrightarrow \sum_{k=r}^{N} \alpha_k = 0 \tag{30}$$

$$\frac{\partial \mathcal{L}}{\partial e_k} = 0 \Longrightarrow \alpha_k = \gamma e_k, \qquad k = r, \dots, N \tag{31}$$

$$\frac{\partial \mathcal{L}}{\partial \alpha_k} = 0 \Longrightarrow y_k = (25), \tag{32}$$

$$\frac{\partial \mathcal{L}}{\partial \beta_k} = 0 \Longrightarrow \sum_{k=1}^{N} w_x^{\mathrm{T}} \varphi\big(x_x(k)\big) = 0, \quad x = a_1, a_2, b_1, b_2 \tag{33}$$

Substitute (28), (29) and (30) into (32), the following equations can be obtained respectively

$$\begin{aligned}y(k) = a_0 y_{k-1} + b_0 y_{k-2} + c_1 u_{k-1} + c_2 u_{k-2} + \sum_{t=r}^{N} \alpha_t \, K_{a1}(t,k) + \beta_{a1} \sum_{t=1}^{N} K_{a1}(t,k) + \sum_{t=r}^{N} \alpha_t \, K_{a2}(t,k) \\ + \beta_{a2} \sum_{t=1}^{N} K_{a2}(t,k) + \sum_{t=r}^{N} \alpha_t \, K_{b1}(t,k) + \beta_{b1} \sum_{t=1}^{N} K_{b1}(t,k) + \sum_{t=r}^{N} \alpha_t \, K_{b2}(t,k) \\ + \beta_{b2} \sum_{t=1}^{N} K_{a1}(t,k) + d + e_k \qquad k = r, \dots, N\end{aligned} \tag{34}$$

$$\sum_{k=1}^{N} \sum_{t=r}^{N} \alpha_t \, K_{a1}(t,k) + \beta_{a1} \sum_{k=1}^{N} \sum_{t=r}^{N} K_{a1}(t,k) = 0 \tag{35}$$

$$\sum_{k=1}^{N}\sum_{t=r}^{N}\alpha_t K_{a2}(t,k)+\beta_{a2}\sum_{k=1}^{N}\sum_{t=r}^{N}K_{a2}(t,k)=0 \tag{36}$$

$$\sum_{k=1}^{N}\sum_{t=r}^{N}\alpha_t K_{b1}(t,k)+\beta_{b1}\sum_{k=1}^{N}\sum_{t=r}^{N}K_{b1}(t,k)=0 \tag{37}$$

$$\sum_{k=1}^{N}\sum_{t=r}^{N}\alpha_t K_{b2}(t,k)+\beta_{b2}\sum_{k=1}^{N}\sum_{t=r}^{N}K_{b2}(t,k)=0 \tag{38}$$

Rewrite the above equations into a set of linear equations as follows.

$$\begin{bmatrix} 0 & 0 & 0 & 1^T & 0 \\ 0 & 0 & 0 & Y_p & 0 \\ 0 & 0 & 0 & U_p & 0 \\ 1 & Y_p^T & U_p^T & K+\gamma^{-1}I_N & K^0 \\ 0 & 0 & 0 & K^{0^T} & 1_N^T\Omega 1_N I_{m+1} \end{bmatrix}\begin{bmatrix} d \\ \mathrm{a} \\ \mathrm{c} \\ \alpha \\ \beta \end{bmatrix} = \begin{bmatrix} 0 \\ 0 \\ 0 \\ Y_f \\ 0 \end{bmatrix} \tag{39}$$

Where $\mathrm{a}=[a_0 \quad b_0]$, $\mathrm{c}=[c_1 \quad c_2]$,
$\alpha_k, k=r,\dots,N$, β_x and d can be obtained from the aforementioned linear equations::

Where $Y_f=[y_r \quad \cdots \quad y_N]^T$, $\mathrm{I}_N=[1 \quad \cdots \quad 1]^T$,

$$Y_p=\begin{bmatrix} y_{r-1} & y_r & \cdots & y_{N-1} \\ y_{r-2} & y_{r-1} & \cdots & y_{N-2} \end{bmatrix},$$

$$U_p=\begin{bmatrix} u_{r-1} & u_r & \cdots & u_{N-1} \\ u_{r-2} & u_{r-1} & \cdots & u_{N-2} \end{bmatrix}$$

$$K^0(p,q)=\sum_{k=1}^{N}\Omega_{k,r+p-q}\,,K(p,q)=\sum_{j=0}^{m}\Omega_{p+r-j-1,q+r-j-1}$$

Because the nonlinear dynamic signal is correlated with the noise in the dynamic model, which is assumed to have zero mean and low variance, a Gaussian Radial Basis functional is preferable than alternative kernel functions for data classification (10). Here, we utilize a Gaussian radial basis, and its kernel has the shape below.

$$\Omega = K(x_t,x_k)=exp\left(-\frac{\|x_t-x_k\|^2}{2\sigma^2}\right) \tag{40}$$

Where σ is a deviation constant.

5. Drop Test Experiment and Identification

To prove that the drop standard of the airplane is met, the test rig performs a drop test with the wheel stopped [21]. The landing gear testing apparatus is seen in Figure 5. The landing gear reliability and durability are examined. The drop test requires a platform large enough to support the entire airplane, two rings to hold the airplane in place throughout the test, and a frictionless sliding mechanism connecting the rings to the main platform (Abramowitz et al. [22]). Before beginning the drop test, the starting weight and impact force are measured using three tiny wheel platforms. The load cells are set up under each of the decks. Two light sensors are installed in each primary landing gear to detect how much each wheel and strut are moving in relation to the ground. The data logger takes in a signal from the load cell and the light sensor, analyzes the signal, and then utilizes the processed data to assess the landing gear's motion.

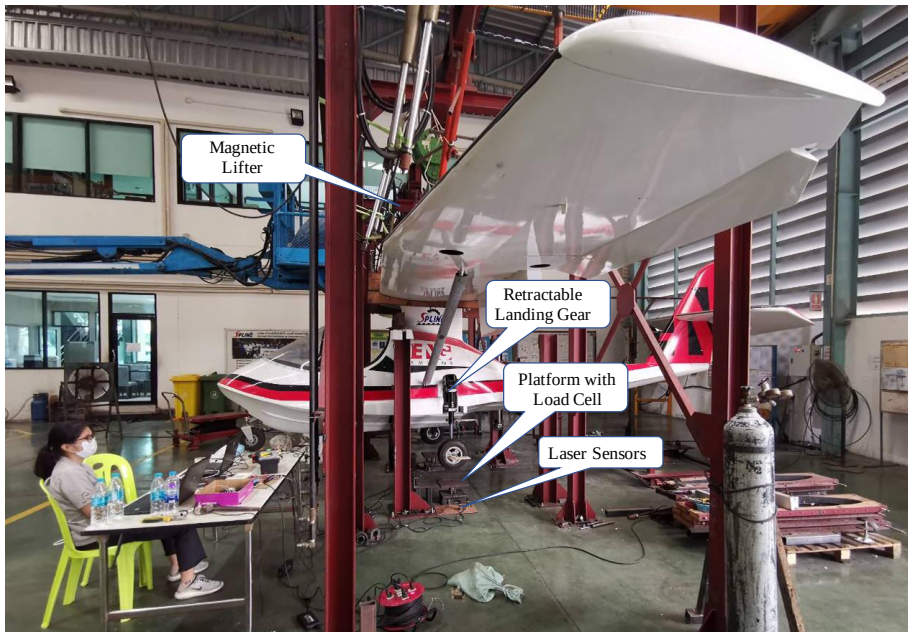

Fig. 5. Drop test rig of a light amphibious airplane.

Using Section 5.8.1 for ASTM 2245, the necessary drop height to verify undercarriage strength is given as $h = 3.6\sqrt{\left(\frac{W}{S}\right)}$, where $\frac{W}{S}$ is wing loading. The load factor is an output from an equation where the distance traveled by the tires and the shocks are inputs. For the tested aircraft, the maximum takeoff weight is 1430 lb (650 kg), and the wing area is 140.85 sq. ft., so the wing loading is equivalent to 10.54 lb/sq. ft., and the highest drop height is 11.69 feet high (approximately 30 cm), and the undercarriage must demonstrate proof of complying with restricted drop height with no detrimental effects.

As can be seen in Table 1, the core component of the drop test experimental setup is a full-body light amphibious airplane. Main wheel tires are inflated at 25 psig, while a nose wheel tire is inflated at 20 psig. Using the charge valve located at the strut's apex, 0.8 MPa. nitrogen gas is pumped into the struts. The light amphibious aircraft's empty weight of 650 kilograms is distributed as follows: 90% on each of the main wheels and 10% on the nose wheel. When the landing gear of an amphibious aircraft is on the deck, the first stroke of both struts is 100 millimeters. The amphibious airplane is lifted up to the proper height for a drop at 20 cm, 25 cm, or 30 cm, and it is dropped through free fall to land on the platform. Tables 2 and 3 show the results of both left and right primary landing gear drop tests at varying drop heights. Highest loads of 831.92 kgf were measured on the left wheel and 813.38 kgf were recorded on the right wheel after being dropped from a height of 200 mm, yielding an impact load factor of nearly 2.53 G. Maximum load in the left and right wheels at a drop height of 25 cm are 1,222.05 kgf and 1,282.90 kgf, respectively, for an actual impact load factor of roughly 3.85 G. At a height of 30 cm, the peak load is 1568.42 kgf on left wheel and 1,555.09 kgf on right gear, for an overall impact load factor of around 4.8 G.

Table 1: Drop test initial parameters.

Airplane Drop Weight	**Wheel Diameter**	**Minimum Strut Stroke**	**Beginning Strut Stroke**	**Gas Pressure *Fill in***	**Retracted oil-hole *Strut Diameter***	**Extened oil-hole Strut Diameter**
650 kg	240 mm	20 mm	100 mm	0.8 Mpa	12 mm	8.5 mm

Table 2: The left main landing gear drop test result.

Main Landing Gear (Left)				
Test Number	**Drop Height**	**Strut Stroke Displacement**	**Tire Deflation Displacement**	**Impact Load**
1	20 cm	56.12 mm	31.73 mm	831.92 kgf
2	25 cm	94.43 mm	47.01 mm	1222.05 kgf
3	30 cm	97.85 mm	52.47 mm	1568.42 kgf

Table 3: The right main landing gear drop test result.

Main Landing Gear (Right)				
Test Number	**Drop Height**	**Strut Stroke Displacement**	**Tire Deflation Displacement**	**Impact Load**
1	20 cm	55.53 mm	28.76 mm	813.38 kgf
2	25 cm	89.51 mm	39.19 mm	1282.90 kgf
3	30 cm	87.78 mm	41.36 mm	1555.09 kgf

Given the sampling rate of 1,000 hertz set by the data collection system, The landing gear must withstand the impact force when dropped from a height of 30 cm, as shown in Figure 6. The data logger recorded a total of 2,000 data points after the drop test was completed in under 2 seconds. Nose gear is obviously not damped, since there is no damping element put where it should be (at the wheel). The mainly two wheels take the brunt of the stress, whereas the nose wheel only experiences a little peak load. Accordingly, the current configuration of the nose wheel is adequate to enduring the impact force it encounters during landing.

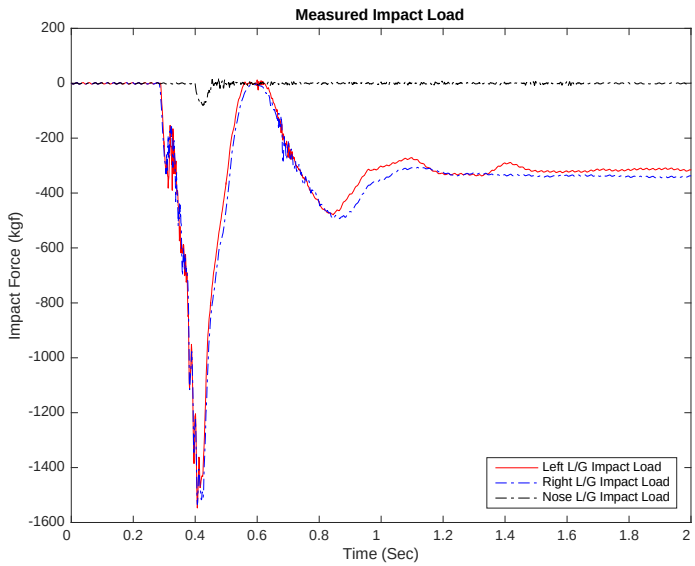

Fig. 6. Force exerted by a drop from 30 centimeters on the nose and main wheels.

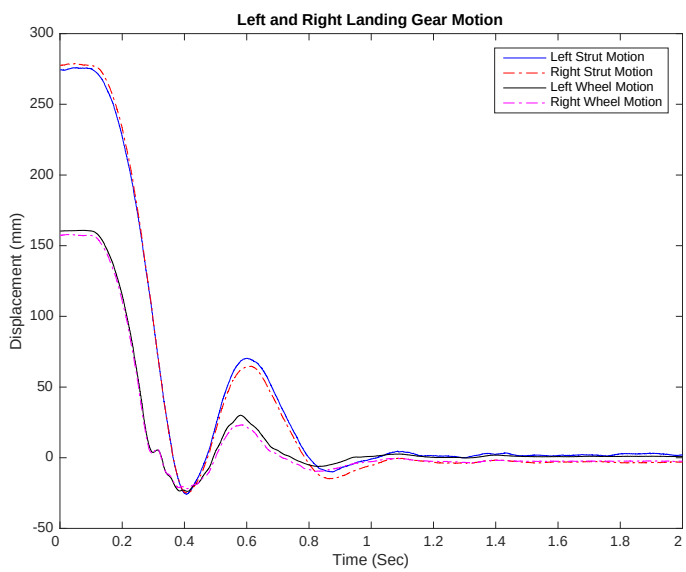

Fig. 7. At a height of 30 centimeters, the relative movement of the main landing gear's strut and wheel was measured.

Figure 7 displays the relative motion of both landing gears' wheels and struts from the start of the drop test forward. An obvious depiction of the settling time associated with the impact force and the whole strokes range of the struts and wheel is shown. Due to the fact that both struts settle in under 2 seconds, this performance ensures the landing gear's reliability and steadiness. Fig. 8 depicts the plane's slow descent, platform impact, and shock strut bounce. A tire dropped from 30 cm will be practically flat at the peak of the impact force, yet the rim remains undamaged when the tire returns to its usual shape.

a) released b) descending c) impacted d) recoiled e) stretched

Fig. 8 the rhythmic motion of a drop test.

The LS-SVM model is trained using the initial 200 input and out impact loads, and displacement data points of strut and wheel. Figure 7 shows that the training data begins when the wheel first touches the platform, indicating a relative drop time of 0.28 seconds. The convex constraint optimization issue is solved using the suggested identification approach and the Gaussian radial basis multi-kernel functional when the KKT condition holds. Parameter values for all of the multi-kernel LS-SVM models are included in Table 4, along with the table itself.

The left and right strut displacements during the drop test are shown graphically in Figures 9 and 10, respectively, on a time scale ranging from 0 to 1 second. There is a comparison between these numbers. The dynamic response from the equation of motion is also shown, along with the identified output from the LS-SVM model with one kernel, the identified output from the LS-SVM model with four kernels, and so on. The preceding section has all of this data. The multiple kernels LS-SVM model clearly delivers the best accurate estimation when checking against the real drop data. The RSME for the left strut is 0.21766, while the RSME for the right strut is 0.30829. Both of these estimates fall well short of the true values for precipitation loss. Single-kernel LS-SVM model RMSE for the right strut is 0.55139, whereas RMSE for the left strut is 0.98941. Using a root-mean-square error (RMSE) metric, we can see that the worst-case identification occurs when comparing the response from the dynamic equation of motion to the actual drop values; in this case, the RMSE is 10.6732 on the right strut and 7.5732 on the left.

Displacements observed in the left and right wheels are shown in Figures 11 and 12, respectively. By comparing the predicted and observed values for each wheel's drop, we can once again show that the multiple kernels LS-SVM model can predict the closest displacement output, with a relative standard deviation of 0.062726 for the left wheel and 0.1584 for the right. When comparing the predicted drop values from the single kernel LS-SVM model to the actual drop values, the RSME is 0.31107 for the left wheel and 0.71204 for the right wheel. The reaction from the dynamic equation of motion deviates from the actual drop values by an RSME of 8.0957 for the left wheel and 6.5626 for the right wheel.

Table 4: Parameter of single/multiple kernels LS-SVM.

Parameter of Single Kernel LS-SVM		**Parameter of Multiple Kernels LS-SVM**	
Strut	***Wheel***	***Strut***	***Wheel***
a_0 = 0.3726	a_0 = 0.4731	a_0 = 0.3936	a_0 = 0.4247
b_0 = 0.6135	b_0 = 0.5116	b_0 = 0.5752	b_0 = 0.5660
c_1 = 0.0298	c_1 = 0.0110	c_1 = 0.0127	c_1 = 0.0087
c_2 = 0.0267	c_2 = -0.0105	c_2 = -0.0154	c_2 = -0.0084

Since struts are nonlinear in terms of axial load and have complicated internal construction structures, we can safely say that they are not as easily identifiable as wheels. However, the identified multiple kernel LS-SVM model proves

more accurate than the single kernel LS-SVM model, both models will still have error rates well within the allowable ranges, allowing them to be used to predict the aircraft's drop dynamics in scenarios where they are not explicitly tested.

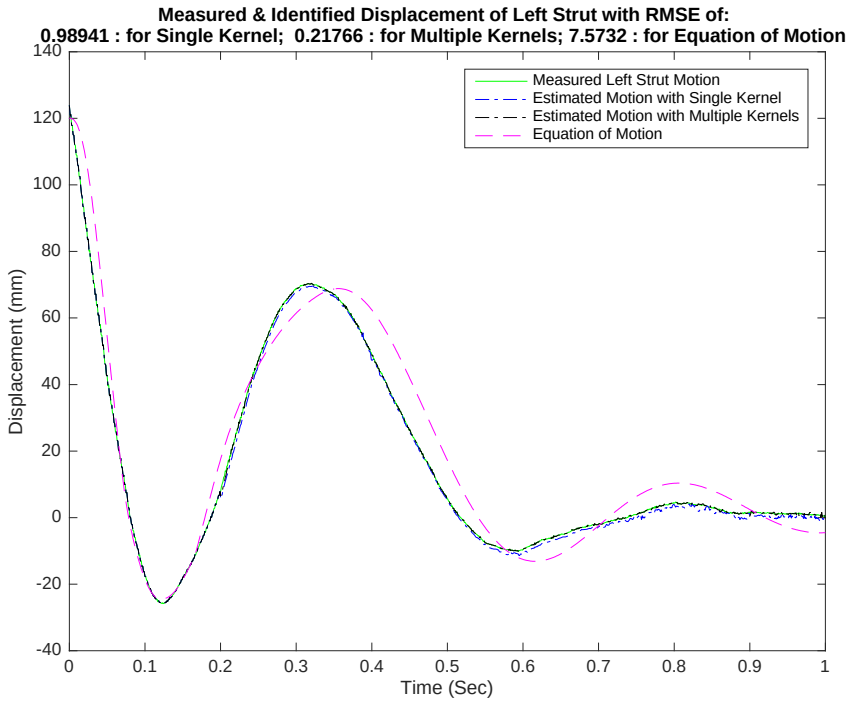

Fig. 9. Measured and identified displacement of the left strut.

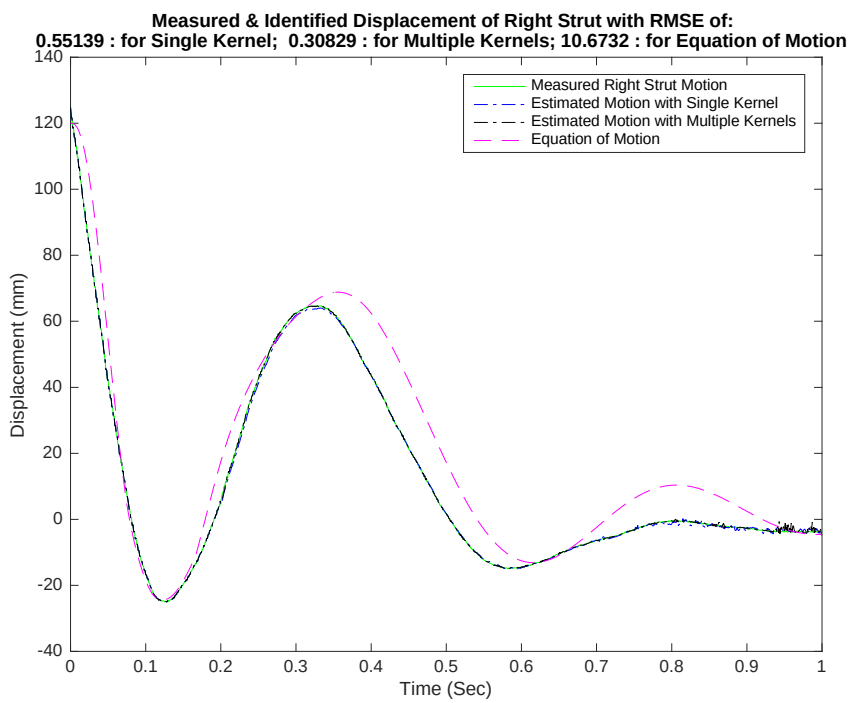

Fig. 10. Measured and identified displacement of the right strut.

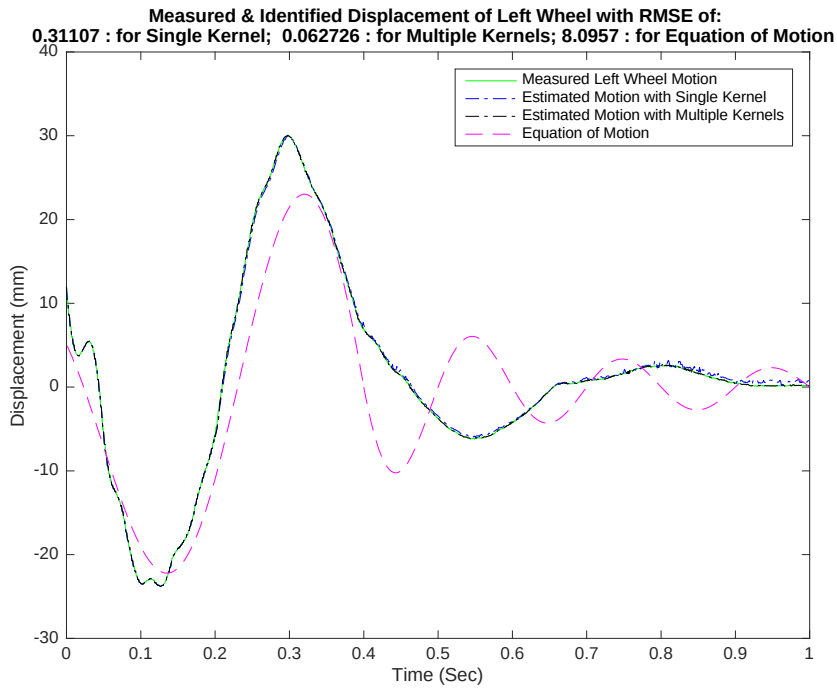

Fig. 11. Measured and identified displacement of the left wheel.

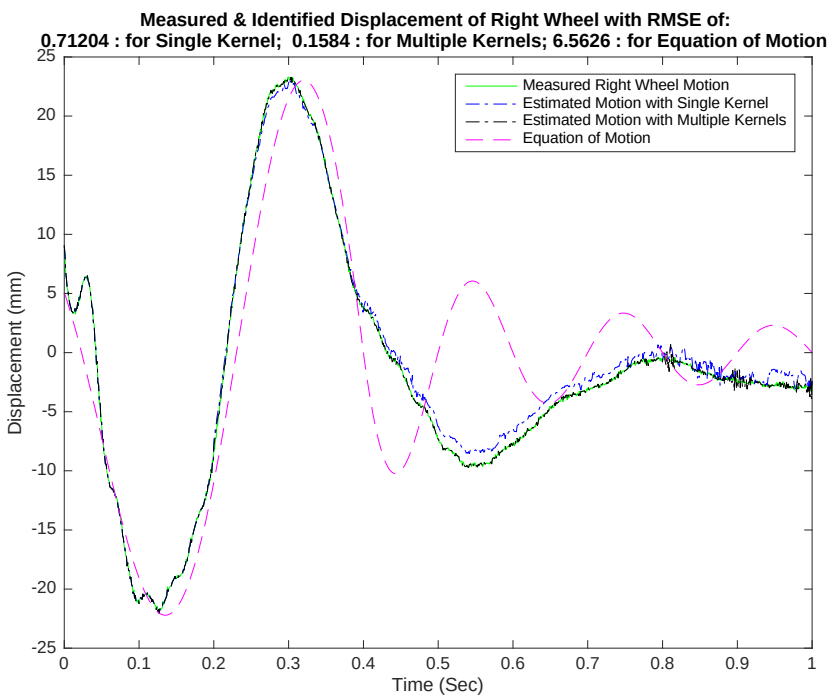

Fig. 12. Measured and identified displacement of the right wheel.

6. Conclusion

To analyze the landing gear's dynamics, an LS-SVM multi-kernel identification model has been created. Combining a series of multi-kernel training modules with an LS-SVM identification module forms the identified model. The model parameters are determined by formulating a constraint convex optimization problem and solving it with the

KKT condition, where the kernel function is the Gaussian radial basis used to predict the nonlinearity of the system. It has been demonstrated that the multi-kernels LS-SVM model yields more accurate recognized displacement output than the traditional kernel model.

In accordance with ASTM F-2245, the full-scale drop test study is carried out on a lightweight amphibious airplane. When dropped from a height of 30 centimeters, the maximum impact loading is 4.8 G. In less than 2 seconds after impact, the main landing gear's shocks strut has neutralized the momentum of impact and restored the plane's equilibrium. The LS-SVM using multi-kernel identifying is suggested for forecasting strut and wheel movement outputs since it outperforms both the identification single-kernel LS-SVM as well as the estimates from the governing equations of motion.

Acknowledgments

The author wishes to thank Pongsak HONGNGERN, CEO of Spline Engineering and Construction Co., Ltd., as well as the company's support staff, for their contributions to the development of the test rig that was utilized in this work. The Department of Mechanical and Aerospace Engineering, King Mongkut's University of Technology and National Business (KMUTNB), and Thailand Science Scientific and Innovation (TSRI) are also appreciated for their research cooperation, technical help, and financial support during the project.

Nomenclature

A_1	inner trans area of the rod, m^2
A_2	outer trans area of the rod, m^2
A_a	compressed air area, m^2
A_h	hydraulically area, m^2
C_d	discharge coefficient
C_T	tire vertical damping coefficient
p_{a_0}	gas pressure for a fully expanded strut, N/m^2
$p_h - p_a$	differential pressure across the orifice, N/m^2
$f(\delta)$	tire static compression function
F_1	normal force on the upper bearing, N
F_2	normal force on lower bearing, N
F_a	friction force, N
F_f	axial force, N
F_h	pneumatic force, N
s	expansion strokes, mm
V_0	air pressures in the upper chamber, m/s
μ_1	coefficient of friction for upper bearing
μ_2	coefficient of friction for lower bearing
δ	wheel hub axial movement, mm
$\dot{\delta}$	wheel hub axial speed, m/s

References

[1] Curry NS. Airplane landing gear design: principle and practice. Washington: AIAA Education Series; 1988.
[2] Daniels JN. A method for landing gear modeling and simulation with experimental Validation. Contractor Report 201601. Hampton: NASA; 1996.
[3] Vapnik V. Estimation of dependences based on empirical data. Moscow: Nauka; 1979.
[4] Vapnik V. The nature of statistical learning theory. NewYork: Springer-Verlag; 1995.
[5] Cristianini N, Shawe-Taylor J. An introduction to support vector machines and other kernel-based learning method. England: Cambridge University Press; 2000.
[6] Suykens J. Support vector machines: a nonlinear modeling and control perspective. Eur J Control. 2001;7(2-3):311-327.
[7] Suykens J, Van Gestel T, De Brabanter J, De Moor B, Vandewalle J. Least squares support vector machines. Singapore: World Scientific; 2002.

[8] Resendiz-Trejo J, Yu W, Li X. Support vector machine for nonlinear system online identification. 3rd International Conference on Electrical and Electronics Engineering; 2006 Sep 6-8; Veracruz, Mexico. USA: IEEE; 2006. p. 1-4.
[9] Viana F, Steffen V, Zanini M, Magalhaes S, Goes L. Identification of a nonlinear landing gear model using nature-inspired optimization. Shock Vib. 2008;15:257-272.
[10] Tarhouni M, Laabidi K, Lahmari-Ksouri M. System identification based on multi-kernel least square support. Proceedings of the International Conference on Fuzzy Computation and 2nd International Conference on Neural Computation; 2010 Oct 24-26; Valencia, Spain. Portugal: SciTePress; 2010. p. 310-315.
[11] Ding Y, Wei X, Nie H, Li Y. Discharge coefficient calculation method of landing gear shock absorber and its influence on drop dynamics. J Vibroengineering. 2018;20(7):2550-2561.
[12] Chinvorarat S. Weiner model drop test identification of a light amphibious airplane. Eng J. 2022;26(1):25-37.
[13] Chinvorarat S, Watjatrakul B, Nimdum P, Sangeet T, Soontornpasatch T, Vallikul, P. Static testing for composite wing of a two-seater amphibious airplane. IOP Conf Ser: Mater Sci Eng. 2019;501:012026.
[14] Chinvorarat S, Watjatrakul B, Nimdum P, Sangeet T, Soontornpasatch T, Vallikul P. Six-degree of freedom mathematical dynamic model of a light-sport aircraft. IOP Conf Ser: Mater Sci Eng. 2020;886:012011.
[15] Chinvorarat S, Vallikul P. A novel retractable landing gear of a light amphibious airplane design, synthesis, analysis, and implementation. Aircr Eng Aerosp Technol. 2021;93(10):1547-1558.
[16] ASTM. ASTM F2245-20: Standard specification for design and performance of a light-sport airplane. West Conshohocken: ASTM; 2020.
[17] Milwizky B, Cook EF. Analysis of landing-gear behavior. Report NACA-TN-2755. USA: NACA; 1952.
[18] Wang XD, Ye MY. Nonlinear dynamic system identification using least squares support vector machine regression. Proceedings of 2004 International Conference on Machine Learning and Cybernetics; 2004 Aug 26-29; Shanghai, China. USA: IEEE; 2004. p. 941-945.
[19] Jing S. Identification of a deterministic wiener system based on input least squares algorithm and direct residual method. Int J Model Identif Control. 2020;34(3):208-216.
[20] Sonnenburg S, Ratsch G, Schfer C, Schlkopf B. Large scale multiple kernel learning. J Mach Learn Res. 2006;7:1531-1565.
[21] Xue CJ, Han Y, Qi WG, Dai JH. Landing-gear drop-test rig development and application for light airplanes. J Aircr. 2012;49(6):2064-2076.
[22] Abramowitz A, Ingraham PA, McGuire R. Vertical drop test of a shorts 3-30 airplane. DOT/FAA/AR-99/87. Washington: Office of Aviation Research; 1999.